INTERNATIONAL JOURNAL FOR NUMERICAL AND ANALYTICAL METHODS IN GEOMECHANICS, VOL. 20, 887–905 (1996)

FINITE ELEMENT MODELLING OF A DEEP SEA CLAY IN LONG-TERM LABORATORY CREEP TESTS

H. G. BRANDES

Department of Civil Engineering, University of Hawaii, Honolulu, HI, U.S.A.

AND

M. H. SADD AND A. J. SILVA

Marine Geomechanics Laboratory, University of Rhode Island, Narragansett, RI, U.S.A.

SUMMARY

A new finite element program is introduced and its predictive capabilities are compared to results from two long-term, drained laboratory creep tests on a deep sea clay. The constitutive behaviour is based on Cam clay critical state plasticity theory with creep and time-dependent hardening. Creep is computed using either Singh–Mitchell's three-dimensional equation or Taylor's secondary compression relationship. The experimental creep data include a triaxial specimen subjected to two deviatoric stress increments and a one-dimensional consolidation specimen subjected to three vertical stress increments. In addition, the pore pressure behaviour following an increase in stress is examined in the triaxial sample. Predictions compare favourably to test data, which provide confidence for applying the chosen constitutive model and numerical formulation to solve seabed-related problems on the continental slope that are of interest to geologists, the oil industry and the navy, among others.

KEY WORDS: creep; modelling; long-term; triaxial; drainage; marine clay

INTRODUCTION

Most fine-grained marine sediments are highly flocculated, have large void ratios and low permeabilities, and are easily deformed even under low stresses. Creep and stress relaxation can constitute a significant component of the overall stress–strain–time behaviour.[1,2] Interest in modelling the behaviour of these sediments has been increasing as seafloor utilization spreads to deeper water where fine-grained deposits are more common. Of particular interest are the continental slope and rise where geologists have identified specific morphological features interpreted to be associated with long-term viscoplastic deformations.[3] There is evidence to suggest that some of the massive slope failures observed on acoustic records were preceded by creep. Oil companies have begun studies to quantify the effect that time-dependent deformations can have on large structures that have either been installed or are contemplated at various locations on the continental slope. The work presented here originated from some of these studies and represents an initial effort to develop and test a comprehensive numerical capability to accurately model the behaviour of fine-grained marine sediments.

In parallel to the development of a new finite element code, GEO-CP, a comprehensive testing program is also being conducted to determine the engineering properties of marine sediments from continental margins and the deep ocean. A number of long-term, drained triaxial creep tests have been conducted at various stress levels lasting from a few weeks to over a year.[1,2,4,5] In

CCC 0363–9061/96/120887–19

Received 24 July 1995
Revised 30 May 1996

addition to creep tests, a large database exists on stress–strain, strength, permeability, and consolidation chracteristics of sediments from various locations in the North Atlantic, North Pacific and Gulf of Mexico.[6-8] These data provide a unique opportunity to evaluate the new code by comparing long-term laboratory test results to predictions under conditions that simulate the quasi-static environment existing at many seabed locations. We concentrate on two drained creep tests conducted on undisturbed samples of a deep sea clay from the North Central Pacific. This site has been studied extensively in the past as part of the Department of Energy's Subseabed Disposal Program and the constitutive parameters are well known. The first test is a two-stage drained, triaxial creep test, lasting 94 days, while the second experiment is a three-stage one-dimensional creep test lasting 110 days. The focus is on the long-term behaviour, which is of special interest to many geologic and engineering applications.

In addition, the pore pressure response in the triaxial specimen is investigated following an increase in the applied stress. Two-dimensional drainage results in inhomogeneous stresses which can be quite different from the applied stresses. A useful application of this type of modelling is in selecting appropriate load schedules for drained triaxial creep tests, where one is typically interested in minimizing inhomogeneities.

CONSTITUTIVE BEHAVIOUR AND FEM FORMULATION

The constitutive model implemented in GEO-CP combines critical state plasticity[9] with creep and hardening, along the lines of the stress stress–strain–time model proposed by Borja and Kavazanjian.[10] Only the main features and equations of this model are presented here.

Central to the formulation is the assumption that the strain tensor can be decomposed into an immediate portion (elastic, ε^e, and plastic, ε^p) and a time-dependent (creep, ε^t) component:

$$\dot{\varepsilon}_{kl} = \dot{\varepsilon}^e_{kl} + \dot{\varepsilon}^p_{kl} + \dot{\varepsilon}^t_{kl} \tag{1}$$

The constitutive model characterizes the behaviour of the solid phase, hence all stresses and material parameters are effective quantities.

Time-independent deformation is characterized by critical state strain-hardening elastoplasticity. The projection of the state boundary surface onto the $(p–q)$ plane is given by the modified Cam clay yield function:

$$F = \frac{q^2}{M^2} + p(p - p_c) \tag{2}$$

where q and p are the generalized three-dimensional deviatoric and volumetric stress quantities, M is the slope of the critical state line (CSL) and p_c is the preconsolidation stress. The projection onto the e–$\ln p$ plane coincides with the virgin isotropic consolidation line:

$$e = e_a - \lambda \ln p_c \tag{3}$$

where λ is the virgin compression index in natural log scale and e_a is the void ratio at $p = 1{\cdot}0$ on the virgin isotropic consolidation line. The state boundary also intersects the CSL, which represents the ultimate failure state. The CSL is given by the two equations

$$q = Mp \tag{4}$$

$$e = e_c - \lambda \ln p \tag{5}$$

where e_c is the void ratio at $p = 1{\cdot}0$ on the CSL. Borja and Kavazanjian also assume that the trace of the Cam clay surface on the deviator stress–shear strain $(q–\gamma)$ plane is given by Kondner's[11]

hyperbolic relationship:

$$q = \frac{\gamma p_c}{a + b\gamma} R_f \tag{6}$$

where a, b and R_f are material constants derived from CIU strength tests with pore pressure measurements.

Formulation of the general constitutive relationship requires use of the associated flow rule on $\dot{\varepsilon}_{kl}^p$:

$$\dot{\varepsilon}_{kl}^p = \phi \frac{\partial F}{\partial \sigma_{kl}} \tag{7}$$

with the consistency requirement on the yield function F such that

$$\dot{F} = \frac{\partial F}{\partial \sigma_{ij}} \dot{\sigma}_{ij} + \frac{\partial F}{\partial p_c} \dot{p}_c = 0 \tag{8}$$

and a hardening rule which describes the growth of the yield function due to plastic volumetric strain and time-dependent effects:

$$\dot{p}_c = \frac{1 + e}{\lambda - \kappa} p_c \dot{\varepsilon}_v^p + \frac{\psi}{\lambda - \kappa} \frac{p_c}{t_v} \tag{9}$$

where $\psi = C_\alpha / \ln 10$ is the coefficient of secondary compression in natural log scale, κ is the recompression index, also in natural log scale, and t_v is the volumetric age, which measures the void ratio distance of a particular point relative to its position on the normally consolidated line:

$$t_v = t_{v_i} \exp(\Delta e / \psi) \tag{10}$$

The factor t_{v_i} is a reference time, usually taken as unity.

Creep strains $\dot{\varepsilon}_{kl}^c$ are obtained by using the normality condition on an equivalent yield surface passing through the current stress state. In our current formulation the magnitude of creep is given either by Taylor's[12] equation for the rate of secondary compression or by Singh–Mitchell's[13] phenomenological creep relationship. For general stress increments, creep strains are scaled off according to the normality rule using Taylor's equation

$$\dot{\varepsilon}_{kl}^c = \frac{\psi}{(1 + e)(2p - p_0) t_v} \frac{\partial F}{\partial \sigma_{kl}} \tag{11}$$

or Singh–Mitchells' equation

$$\dot{\varepsilon}_{kl}^c = \sqrt{\frac{3}{2}} A e^{\alpha D} \left[\frac{t_{d_i}}{t_d}\right]^n \left[\frac{\partial F}{\partial \sigma_{pq}} \frac{\partial F}{\partial \sigma_{pq}} - \frac{1}{3}\left(\frac{\partial F}{\partial p}\right)^2\right]^{-1/2} \frac{\partial F}{\partial \sigma_{kl}} \tag{12}$$

where A, α and m are material parameters derived from triaxial creep tests, D is the stress level given by

$$D = \frac{q}{(0{\cdot}5)^{(1-\kappa/\lambda)} M p_c} \tag{13}$$

and t_d is the deviatoric age, which is a measure of the shear strain, γ, that develops at constant q:

$$t_d = \left[\frac{(\gamma_1 - \gamma_2)(1-m)}{Ae^{\alpha D}(t_{d_i})^m}\right]^{1/(1-m)} \quad \text{if } m \neq 1 \tag{14}$$

$$t_d = t_{d_i}\exp\left(\frac{\gamma_1 - \gamma_2}{Ae^{\alpha D}}\right) \quad \text{if } m = 1 \tag{15}$$

where γ_1 is the total accumulated shear strain due to time-independent and time-dependent deformation, and γ_2 is the shear strain for normally consolidated loading as given by Kondner's hyperbolic law. Again, t_{d_i} is a reference time, usually taken as unity. For this study creep strains were derived using Singh–Mitchell's equation unless noted otherwise.

Using equations (1) and (6)–(9) the following creep-inclusive constitutive relationship is derived:

$$\dot{\sigma}_{ij} = C^{ep}_{ijkl}\dot{\varepsilon}_{kl} - C^{ep}_{ijkl}\dot{\varepsilon}^{t}_{kl} - \frac{\dfrac{\partial F}{\partial p_c}\left(\dfrac{\psi}{\lambda-\kappa}\right)\dfrac{p_c}{t_v}C^{e}_{ijkl}}{\dfrac{\partial F}{\partial \sigma_{mn}}C^{e}_{mnkl}\dfrac{\partial F}{\partial \sigma_{kl}} - \dfrac{\partial F}{\partial p_c}\dfrac{\partial F}{\partial p}\left(\dfrac{1+e}{\lambda-\kappa}\right)p_c}\frac{\partial F}{\partial \sigma_{kl}} \tag{16}$$

where C^{ep}_{ijkl} is the modified Cam clay elastoplastic constitutive tensor. The finite element formulation in GEO-CP uses Biot's[14] three-dimensional equations of consolidation (equilibrium, effective stress principle, Darcy's law and continuity) and the above constitutive relation. The application of virtual work and finite element approximation procedures leads to the following set of incremental, coupled equations:

$$\begin{aligned} \mathbf{K}\Delta\mathbf{u}_{(a)} + \mathbf{L}\Delta\mathbf{w}_{(b)} &= \Delta\mathbf{F} \\ \mathbf{L}^{T}\Delta\mathbf{u}_{(a)} - \Phi\beta\Delta t\Delta\mathbf{w}_{(b)} &= \Delta\mathbf{H} + \Phi\Delta t\mathbf{w}|_{t=t_n} \end{aligned} \tag{17}$$

These equations have been integrated in time using the β family approximation, with β being an input variable ranging between 0 and 1. For all the runs reported here β was set to 0·5 in order to achieve optimum accuracy as well as unconditional stability.[15] Also, t is time and $\mathbf{u}$ and $\mathbf{w}$ are the unknown nodal displacements and pore pressures; $\mathbf{K}$, $\mathbf{L}$ and Φ are the displacement, pore pressure and cross stiffness matrices:

$$\mathbf{K} = \int_{\Omega}\mathbf{B}^{T}\mathbf{C}\mathbf{B}\,d\Omega \tag{18}$$

$$\mathbf{L} = \int_{\Omega}\mathbf{B}^{T}\mathbf{m}\bar{\mathbf{N}}\,d\Omega \tag{19}$$

$$\Phi = \frac{1}{\gamma_w}\int_{\Omega}\mathbf{E}\mathbf{k}\mathbf{E}\,d\Omega \tag{20}$$

$$\mathbf{m} = [1,\ 1,\ 1,\ 0] \tag{21}$$

$$\mathbf{k} = \begin{bmatrix} k_x & 0 \\ 0 & k_y \end{bmatrix} \tag{22}$$

$$\mathbf{E} = \begin{bmatrix} \dfrac{\partial\bar{\mathbf{N}}}{\partial x} & \dfrac{\partial\bar{\mathbf{N}}}{\partial y} \end{bmatrix} \tag{23}$$

$\mathbf{N}$ and $\bar{\mathbf{N}}$ are the displacement and pore pressure approximating functions, $\mathbf{B}$ is the strain-displacement matrix, and k_x and k_y are the horizontal and vertical permeabilities. $\Delta\mathbf{F}$ is the external load and creep relaxation vector and $\Delta\mathbf{H}$ is the seepage vector:

$$\Delta\mathbf{F} = \int_\Omega \mathbf{N}^T \Delta\mathbf{b}\, d\Omega + \int_\Gamma \mathbf{N}^T \Delta\hat{\mathbf{t}}\, d\Gamma + \int_\Omega \mathbf{B}^T \Delta\sigma^t\, d\Omega \tag{24}$$

$$\Delta\mathbf{H} = \int_\Omega \mathbf{N}^T \Delta v\, d\Omega \tag{25}$$

$\mathbf{b}$ and $\hat{\mathbf{t}}$ are the body weight and traction vectors. The stress relaxation term σ^t includes the last two terms in constitutive equation (16). Note that the effect of creep is introduced as an additional forcing term on the right-hand side of equations (17). Treating creep as a pseudo-force allows us to solve problems where the external physical loads do not change. Finally, v is the external seepage normal to the boundary.

Equations (17) represent a set of non-linear equations that need to be solved iteratively until balance is achieved between external and internal nodal forces:

$$\mathbf{F}_{ext} - \mathbf{F}_{int}(\mathbf{D}^*) = \mathbf{0} \tag{26}$$

where $\mathbf{D}^*$ is the assembled vector of nodal displacements and pore pressures that satisfies equilibrium.[16] Given the coupled nature of the consolidation process, it is necessary to satisfy both total momentum balance (at any time t_{n+1}) and incremental mass balance (over any time interval t_n to t_{n+1}) in order to ensure convergence to the correct solution. Momentum and mass balance can be satisfied by expressing the nodal force vectors in equation (26) according to:[16]

$$\mathbf{F}_{ext_{n+1}} = \begin{Bmatrix} \mathbf{F}_{n+1} \\ \Delta\mathbf{H}_n \end{Bmatrix} \tag{27}$$

$$\mathbf{F}_{int_{n+1}}^{k+1} = \begin{Bmatrix} \displaystyle\int_\Omega \mathbf{B}^T \sigma_{n+1}^{k+1}\, d\Omega + \int_\Omega \mathbf{B}^T \omega_{n+1}^{k+1}\, d\Omega \\ \mathbf{L}^T(\mathbf{u}_{n+1}^{k+1} - \mathbf{u}_n) - \Phi\beta\,\Delta t(\mathbf{w}_{n+1}^{k+1} - \mathbf{w}_n) + \Phi\,\Delta t\,\mathbf{w}_n \end{Bmatrix} \tag{28}$$

where subscripts indicate increment number and superscripts stand for iteration number. $\mathbf{F}_{n+1}$ is the vector of applied nodal forces and ω represents the integration point pore pressures. Note that whereas $\mathbf{F}_{ext_{n+1}}$ remains constant for a given time increment, $\mathbf{F}_{int_{n+1}}$ is a function of the unknown displacements and pore pressures $\mathbf{D}_{n+1}^{k+1}$, and is updated in each iteration. The Newton–Raphson method is used to solve equations (26) and is implemented as shown in Table I. Convergence of the solution is monitored using the L_2-norm force criterion

$$\| \mathbf{F}_{ext_{n+1}} - \mathbf{F}_{int_{n+1}}^{k+1} \|_2 \leqslant \varepsilon_F \| \mathbf{F}_{ext_{n+1}} - \mathbf{F}_{ext_{n+1}}^{0} \|_2 \tag{29}$$

and the L_2-norm displacement criterion

$$\| \Delta\mathbf{D}_{n+1}^{k+1} \|_2 \leqslant \varepsilon_D \| \Delta\mathbf{D}_{n+1}^{0} \|_2 \tag{30}$$

subject to minimum and maximum number of iterations. A minimum of two iterations are necessary for the displacement criterion to be meaningful.

Table I. Newton–Raphson iteration algorithm for time increment t_{n+1}: $[t_n \rightarrow t_{n+1}]$

1. Set iteration counter $k = 0$
2. Update applied loads

$$\mathbf{F}_{\text{ext}_{n+1}} = \mathbf{F}_{\text{ext}_n} + \Delta\mathbf{F}_{\text{ext}_{n+1}}$$

3. Let

$$\mathbf{D}^0_{n+1} = \mathbf{D}^*_n \quad \text{and} \quad \sigma^0_{n+1} = \sigma^*_n$$

4. Compute initial force residual

$$\text{ENORM}\,\phi = \|\mathbf{F}_{\text{ext}_{n+1}} - \mathbf{F}^0_{\text{ext}_{n+1}}\|_2$$

5. Compute $\mathbf{C}^k_{n+1}$ (elastic or plastic depending on stress state σ^k_{n+1})
6. Assemble global stiffness matrix $\mathbf{C}^k_{n+1} \rightarrow \mathbf{K}^k_{n+1}$
7. Solve incremental equations

$$\Delta\mathbf{D}^k_{n+1} = \mathbf{K}^{k\,-1}_{n+1}(\mathbf{F}_{\text{ext}_{n+1}} - \mathbf{F}^k_{\text{int}_{n+1}})$$

8. Update displacements and stresses

$$\mathbf{D}^{k+1}_{n+1} = \mathbf{D}^k_{n+1} + \Delta\mathbf{D}^k_{n+1}$$

$$\Delta\varepsilon^{k+1}_{n+1} = \mathbf{B}\,\Delta\mathbf{D}^k_{n+1}$$

$$\sigma^{k+1}_{n+1} = \sigma^k_{n+1} + \mathbf{C}^k_{n+1}\Delta\varepsilon^{k+1}_{n+1}$$

9. Compute new force residual

$$\text{ENORM} = \|\mathbf{F}_{\text{ext}_{n+1}} - \mathbf{F}^{k+1}_{\text{ext}_{n+1}}\|_2$$

10. Compute incremental displacement norm

$$\text{DNORM} = \|\Delta\mathbf{D}^{k+1}_{n+1}\|_2 \rightarrow \text{DNORM0 if } k = 0$$

11. Calculate convergence errors

$$\varepsilon_F = \|\mathbf{F}_{\text{ext}_{n+1}} - \mathbf{F}^{k+1}_{\text{ext}_{n+1}}\|_2, \quad \varepsilon_D = \text{DNORM/DNORM0}$$

12. If less than minimum number of iterations, then $k = k + 1$, go to 5
13. If equal to maximum number of iterations check (a) or (b)
    (a) If no creep during increment
        If $\varepsilon_F <$ force tolerance, go to 15
    (b) If creep is allowed during increment
        If $\varepsilon_D <$ displacement tolerence, go to 15
14. No convergence, stop
15. Next time increment, go to 1

This solution algorithm was highly effective for the triaxial and one-dimensional problems presented below, to a large degree because most of the stresses remained in the elastic range (due to initial overconsolidation and subsequent time-dependent hardening). Convergence was achieved rapidly in all time increments, with values for ε_F and ε_D droping below the 14-digit double-precision resolution of the computer within no more than three or four iterations. More sophisticated solution techniques based on consistent linearization procedures combined with various stress integration methods have been shown to be more effective in problems involving significant plastic straining.[16,17]

GEO-CP[18] was modified from an earlier version of the code CRISP[19] to include the above creep-inclusive constitutive model and the incremental-iterative solution procedure. In its current

version, it allows for the solution of plane strain and axisymmetric problems. The formulation is based on small deformation theory, although the nodal coordinates can be updated after each increment. GEO-CP has shown excellent agreement with theory for a number of elastic problems such as various plane strain plates and footings, comparisons with solutions to Terzaghi's one-dimensional consolidation equation, and Cryer's[20] solution for consolidation of an elastic sphere. We now proceed to test its predictive capabilities in two long-term, drained creep tests. These types of tests are especially relevant to the study of time-dependent deformations in quasi-static submarine slopes where excess pore pressures following a loading or unloading event dissipate rather quickly compared with long geologic time frames.

CONSTITUTIVE PARAMETERS

The laboratory tests discussed below were conducted on an undisturbed, illite-rich deep sea clay from the central North Central Pacific seafloor, in an area 600 miles north of Hawaii known as MPG-I where the water depth is 5800 m. Surface sediments at the site are known as red clays and consist mainly of wind-blown clay materials of various kinds, including fine-grained particles such as quartz, feldspar, pyroxenes, etc. The clay content (<2 μm) is 67%, and the liquid and plastic limits are 92 and 42, respectively. The illite content is about 50% in the less than 2 μm fraction. Gas and organic content are essentially zero. According to Casagrande's plasticity chart, this is an inorganic silty clay of high plasticity. A low sedimentation rate of less than 1 mm per 1000 years produces structural arrangements that are highly flocculated with large void ratios but relatively low permeabilities.

Compressibility, permeability and stress–strain properties in Table II represent the average values from a large number of tests. Consolidation results indicate that the surface sediments at this site are 'apparently' overconsolidated near the surface and approach normally consolidated conditions at 5 m below the seabed.[7] Overconsolidation is attributed to high interparticle bonds and perhaps some cementation rather than overburden removal. Strength and stress–strain parameters were obtained from isotropically and K_0-consolidated triaxial tests with measurement of pore pressure, and in some cases lateral strain. The coefficient of secondary compression was determined from one- and three-dimensional consolidation tests. Since the three Singh–Mitchell parameters were not available from the preliminary testing program, they are instead based on those given by Borja and Kavazanjian[10] for San Francisco Bay mud. Although there is little data correlating creep parameters to physical properties, the very nature of creep in fine-grained sediments suggests that it is a strong function of the plasticity and porosity of the material. Indeed, this red clay from the North Central Pacific has similar Atterberg limits and water content to San Franscisco Bay mud, and might reasonably be expected to have similar creep parameters. The parametric study presented in the next section investigates how the three creep parameters affect the predictions.

EXAMPLE A: DRAINED TRIAXIAL CREEP TEST

The triaxial creep test equipment (Figure 1) and data acquisition system have been developed specifically for conducting long-term tests of soft materials and are explained in detail elsewhere.[1] In the test discussed below the sample was back-pressured to 414 kPa (60 psi), followed by two isotropic consolidation steps, first to 41 kPa (6 psi) and then 93 kPa (13·5 psi). Thus the final effective stress was significantly higher than the vertical preconsolidation stress. The first step was maintained for 4223 min (3 days) and the second one for 2928 min (2 days), both well into the secondary consolidation region. Deviatoric loading was applied by adding dead weight until the

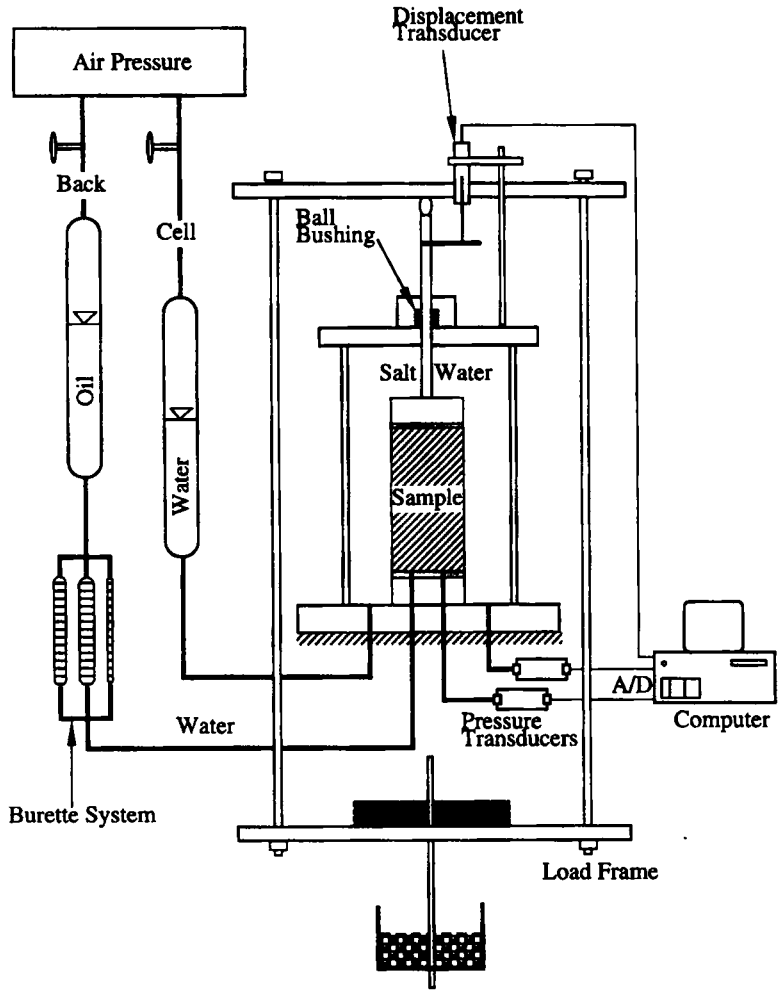

Figure 1. Triaxial creep test apparatus

deviatoric stress reached $q = 34$ kPa, or 20% of the estimated triaxial failure strength, and again later at 60, 130 min (42 days) to reach $q = 68$ kPa, or 40% stress level. Loading was applied in several increments while keeping the drainage valve open to allow for pore pressure dissipation (Figure 2). Axial deformation, cell and back pressure were recorded at regular intervals of at most 45 min. Volume changes were measured from the burette system at least once a day. The deviatoric phase of the test lasted for 133,541 min (93 days).

In the finite element analysis that follows, the upper right-hand quadrant of the cylindrical triaxial specimen is discretized into 112 axisymmetric four-noded isoparametric elements with corner pore pressure nodes for a total of 540 degrees of freedom (Figure 3). Drainage is assumed to occur through the sides, the top and the bottom of the specimen by specifying zero excess pore pressures along those boundaries at all times. We restrict modelling to the deviatoric phase of the test by specifying uniform stress conditions $\sigma_x = \sigma_y = \sigma_z = 93$ kPa, which are in equilibrium with boundary loads of equal magnitude, and by assuming zero excess pore pressures throughout.

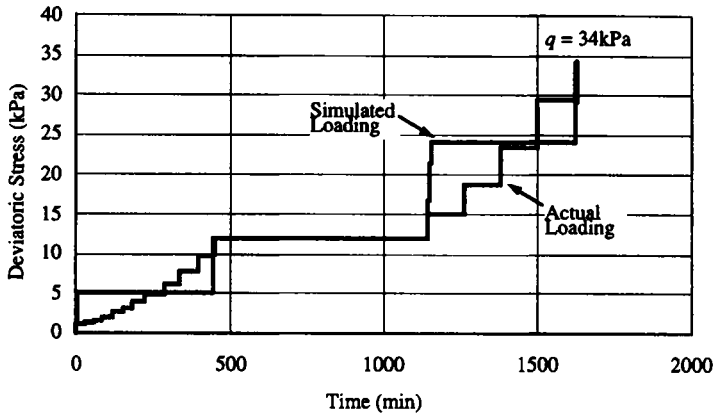

Loading: 0% to 20% of Maximum Deviatoric Stress.

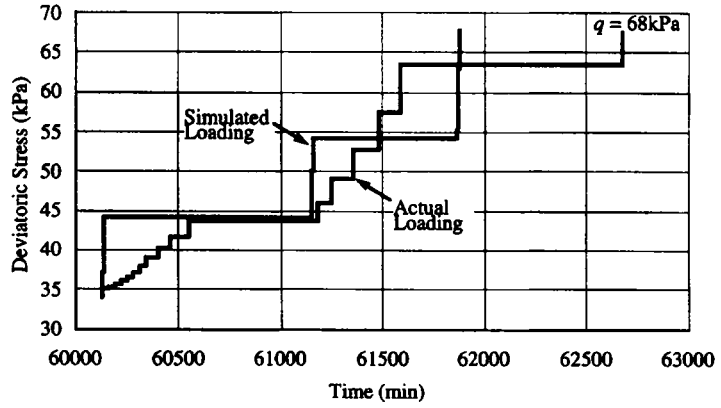

Loading: 20% to 40% of Maximum Deviatoric Stress.

Figure 2. Deviatoric loading of triaxial specimen

Loading is applied to the top and the sample is restrained as shown in Figure 3. Although the simulated loading could have been applied in more than the number of steps shown in Figure 2, preliminary runs indicated that this would not have improved the predictions significantly. Note that for this analysis we assume frictionless ends and thus ignore the lateral restraint imposed by the top and bottom pore stones. Numerical studies by Airey[21] suggest that this type of end condition leads to significantly more uniform stress distributions throughout the specimen, and therefore to closer agreement with Terzaghi's theory. The time increments chosen for the computations ranged from 1 min at the beginning of each deviatoric loading to 681 min at the end. A total of 2280 increments and a minimum of five iterations per increment were used.

As mentioned previously, the deviatoric phase was preceded by isotropic consolidation to 93 kPa, the last step lasting 2928 min (2 days). Since primary consolidation was essentially complete after 275 min, the sample had undergone a significant amount of volumetric creep under constant stress conditions (time-dependent hardening) and was in effect overconsolidated at the beginning of the deviatoric analysis. This results in an initial preconsolidation stress larger than

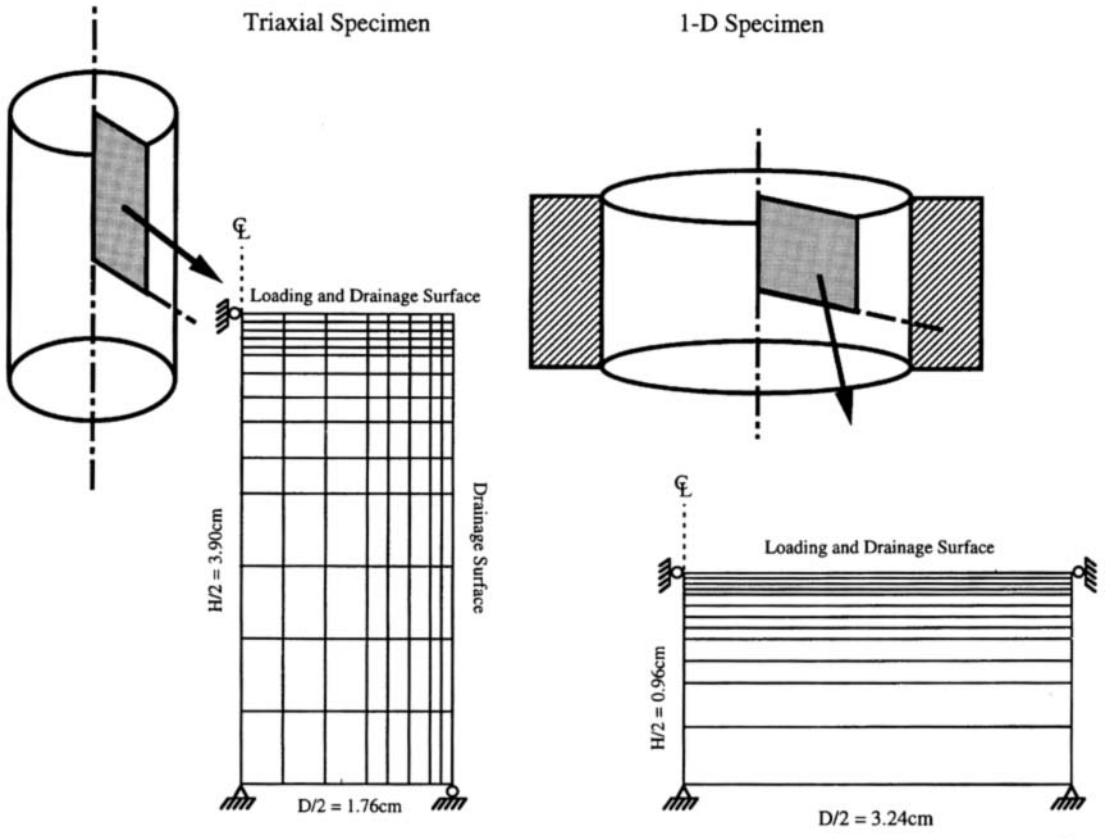

Figure 3. Geometry and mesh

93 kPa, which can be shown to equal:[10]

$$\Delta p_c = p_c \left[\left(1 + \frac{\Delta t_v}{t_v} \right)^{\psi/(\lambda-\kappa)} - 1 \right] = 23\,\text{kPa} \tag{31}$$

$$p_c = 116\,\text{kPa} \tag{32}$$

A comparison between prediction and test results (Figure 4) using the material parameters in Table II and the modelling approach described above shows very good overall agreement in the axial strain at both stress levels. Particularly encouraging to our interest in long-term applications is the excellent agreement in the rate of deformation during secondary compression, after pore pressures have dissipated. The small discrepancy in axial deformation during and immediately following deviatoric loading is attributed in part to the fact that the drainage conditions in the test sample are more restrictive than those used for the model. As shown in Figure 5, predicted pore pressures dissipate quickly near the drainage boundaries. However, in the test drainage through the sides was provided by nine $\frac{1}{2}$ in wide vertical filter strips, which did not fully cover the specimen. A reduced rate of dewatering during primary consolidation would result in lower axial strains when compared to the idealized model predictions, with the differences disappearing after the excess pore pressures have dissipated.

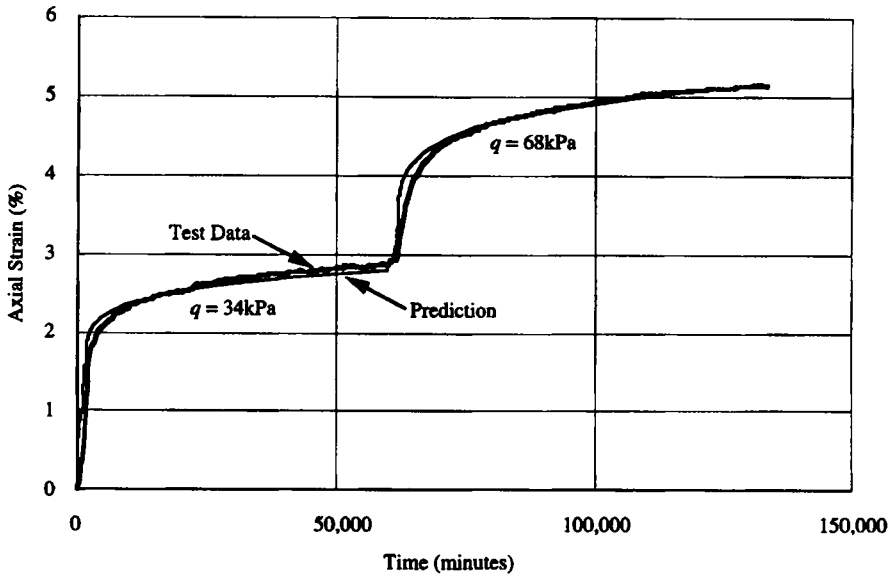

Figure 4. Comparison between triaxial creep test and GEO-CP prediction

Table II. Input material parameters

Parameter		Input value
Poisson's ratio	ν	0·33
Compression index	λ	0·40
Recompression index	κ	0·04
Critical state intercept	e_c	3·41
Critical state slope	M	1·24
Permeability	k	10^{-6} cm/s
Hyperbolic constants	a	0·0072
	R_f	0·95
Secondary compression	Ψ	0·010
Singh–Mitchell constants	A	$0{\cdot}53 \times 10^{-5}$
	m	0·80
	α	4·4

Previous numerical and experimental studies have shown that the generation and dissipation of pore pressures during consolidation can lead to significant inhomogeneities in the triaxial specimen, particularly for the case of combined vertical and lateral drainage.[21-23] Given the relatively low permeability of the material and stress relaxation, the final stress distribution is not as uniform as implied by the applied stress. For example, at the end of the test the applied stresses are $\sigma_x = \sigma_z = 93$ kPa, $\sigma_y = 93 + 68 = 161$ kPa and $\tau_{xy} = 0$ kPa. Thus

$$p = \frac{\sigma_x + \sigma_y + \sigma_z}{3} = 116 \text{ kPa} \tag{33}$$

$$q = \sigma_y - \sigma_x = 68 \text{ kPa} \tag{34}$$

$$\frac{q}{p} = 0{\cdot}59 \tag{35}$$

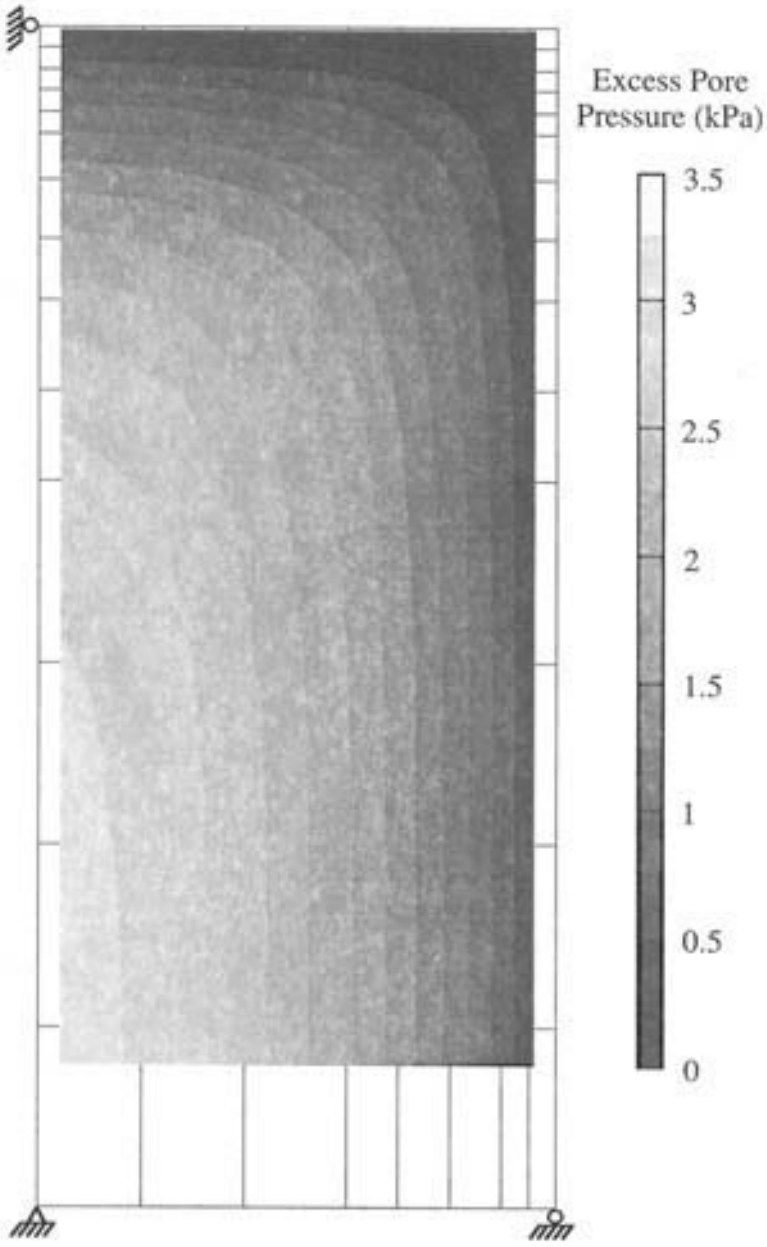

Figure 5. Excess pore pressure at t = 61,940 min (43 days)

The computed q/p ratios (Figure 6) fluctuate around 0·59, with the highest values propagating from the centre of the sample toward the top and right (and due to symmetry to the bottom and left). It is likely that at higher deviatoric stress a failure surface might develop along this plane of high q/p values, from the right top to the bottom left of the sample.

Since the Singh–Mitchell parameters A, α and m require laboratory test data that are time-consuming to obtain, it is of interest to know to what degree they affect the predictions.

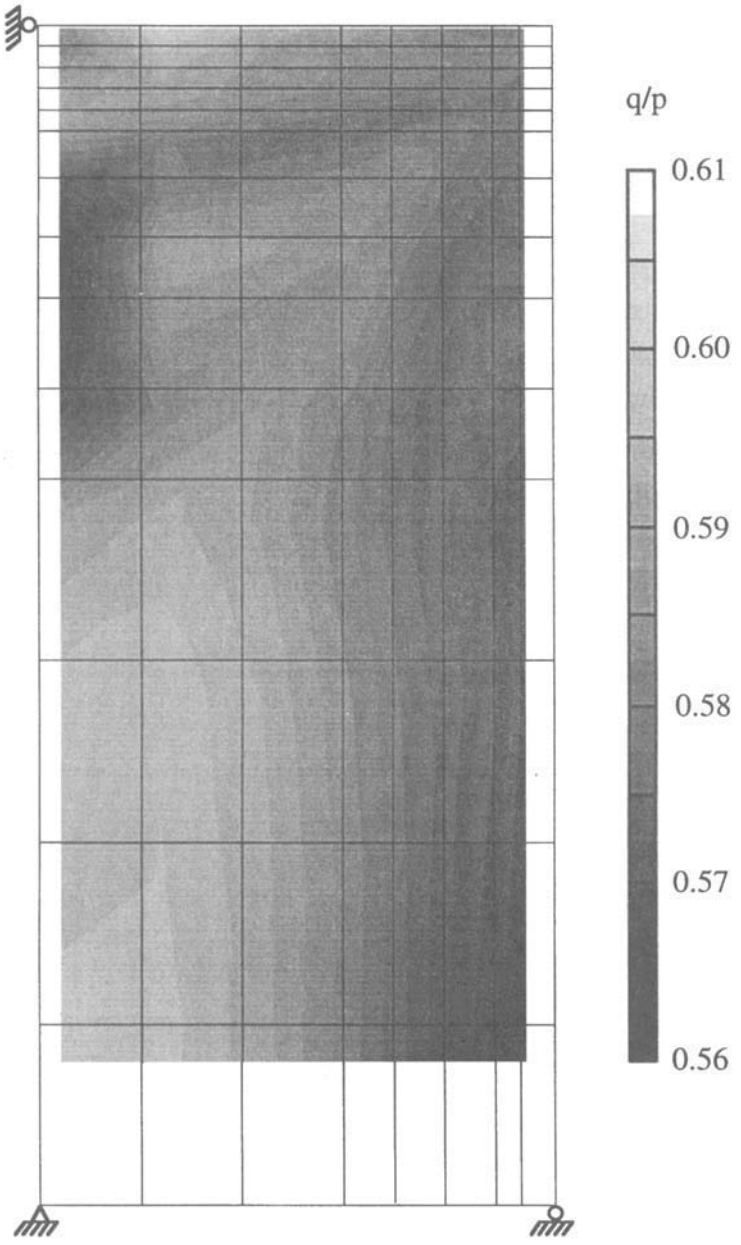

Figure 6. q/p ratios at end of analysis

A sensitivity analysis comparing the first deviatoric stress increment test data with predictions using a constant set of material parameters (slightly different from those in Table II) and various values of A, α and m is shown in Figure 7. The early portion of the predictions, during and immediately after deviatoric loading, is controlled primarily by A and α, whereas the subsequent rate of deformation is dependent on the parameter m, as expected. When considering the

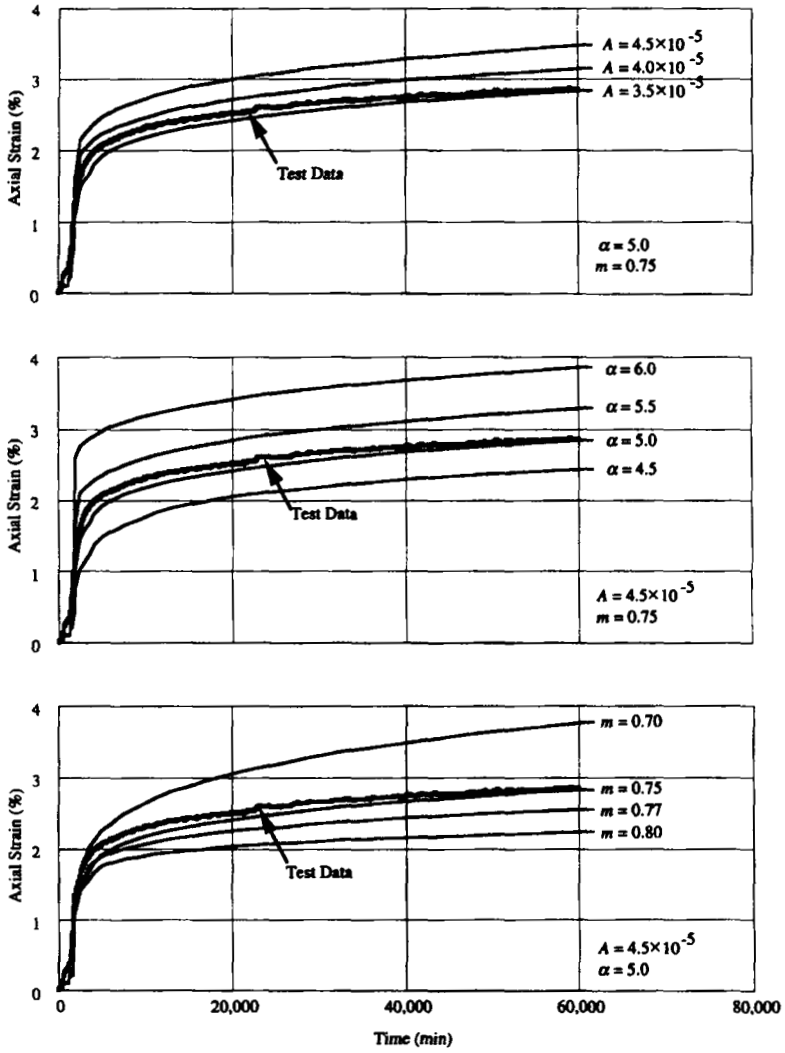

Figure 7. Sensitivity of triaxial predictions to Singh–Mitchell parameters

dependence and sensitivity of the predictions on these parameters it should be remembered that they do not act independently, and when viewed together such dependencies could be considerably less than those shown in Figure 7. There is also experimental evidence to suggest that at least the parameter m is not a constant but instead varies as a function of time[1] and stress level.[5,24]

Numerical simulations were carried out to investigate the response of the triaxial specimen to increase in the confining pressure, i.e. an isotropic stress increase. Although there was good agreement between measured and computed volume changes in the primary region, the predictions tended to overpredict the measured values in the secondary region. This was attributed to unreliable volume change measurements over long periods of time in some of the tests. However, the predictions show that the long-term volumetric strain behaviour for this material is very sensitive to the creep parameters, whereas, as expected, the primary consolidation response is mainly a function of the compressibility and permeability parameters of the material.

EXAMPLE B: PORE PRESSURE RISE/DISSIPATION DUE TO ISOTROPIC COMPRESSION

We can take a closer look at the pore pressure response in the triaxial specimen by considering the second isotropic consolidation step, prior to deviatoric loading. Starting with initial uniform stresses of 41 kPa at the end of the first consolidation step, the cell pressure was increased by an additional 52 kPa. The finite element simulation, using similar material properties to those in Table I and a 48-element mesh, ignores all previous stress history by assuming normally consolidated conditions. Undrained loading ($\Delta p = 52$ kPa) at $t = 0$ is followed by full drainage at $t = 1$ min by specifying excess pore pressures equal to zero along the top and side. Since the initial stress state is on the p-axis, we use Taylor's equation (11) with $\psi = 0{\cdot}01$ to predict the creep strain increments.

The predicted pore pressure response is as shown in Figure 8, where the values have been normalized by the applied stress. Following a uniform rise to 52 kPa due to the undrained

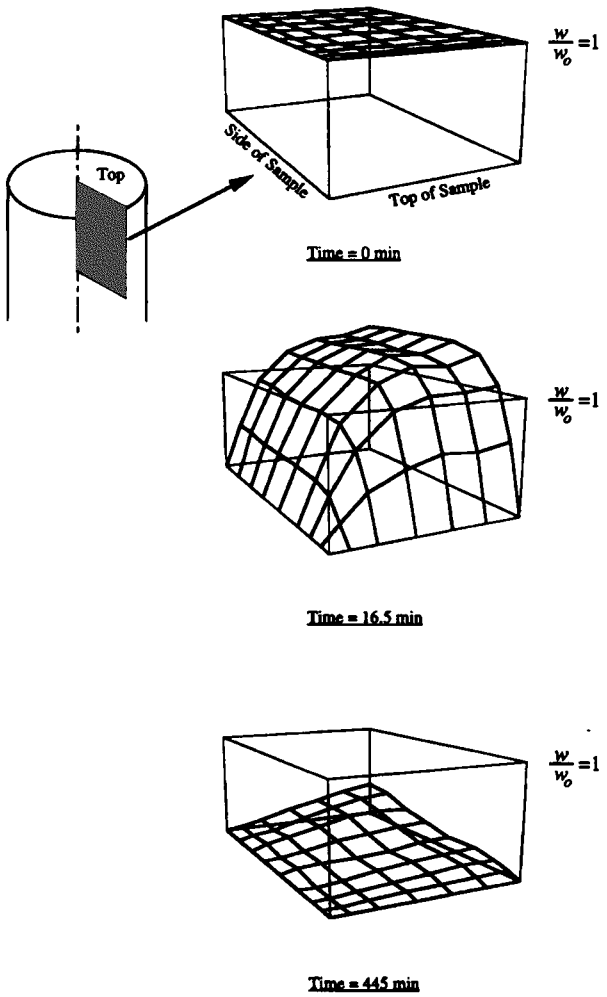

Figure 8. Predicted pore pressure rise and dissipation in triaxial specimen

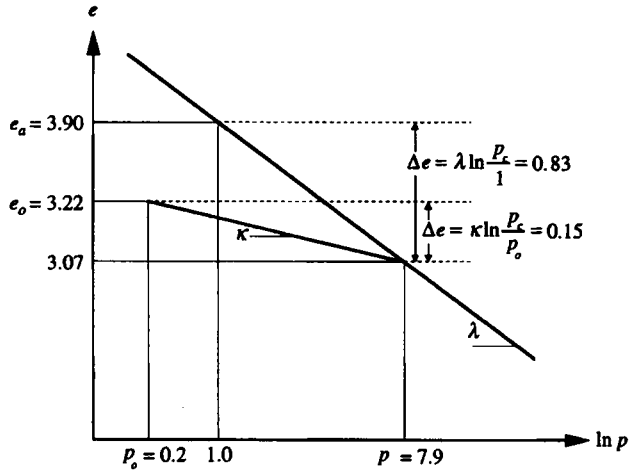

Figure 9. Initial e–ln p state for 1-D creep test

loading, full drainage along the boundaries results in large pore pressure gradients nearby. Meanwhile, the interior of the specimen has not had time to consolidate, and in fact first experiences an increase in pore pressure above 52 kPa before dissipation takes place. This is the well-known Mandel–Cryer effect.[20] Mathematically, it is a consequence of the coupled nature of Biot's equations. Due to continuity, the displacements associated with volume reduction of exterior elements that have begun to consolidate are propagated inward and result in a temporary increase in total stress at locations that have not yet begun to undergo pore fluid migration. Cryer's effect has been observed in a number of numerical as well as experimental studies.[21,25] The fluctuations in excess pore pressure along individual isochrones observed in Figure 8 are associated with the choice of mesh density, element type, and time step size. In particular, element types with a higher-order pore pressure interpolation function or a finer mesh can be expected to better approximate the true shape of the isochrones.

The effect of creep on pore pressure rise and dissipation was also investigated by running the same problem but not allowing for creep or time-dependent hardening. At the centre of the sample, there was little difference in the value of time of occurrence of the maximum pore pressure. In both cases the pressure rose about 40% above the applied stress before starting to decrease. This value is comparable to the theoretical range of 0–57% found by Cryer[20] for an elastic sphere using Poisson's ratios from 0·5 to 0. Once the pore pressures begin to dissipate, they decrease initially at a slower rate for the case with creep. This follows from the added volumetric strain imposed by the creep strain increment, particularly during the early phases of consolidation. Similar results were also observed for deviatoric stress increments.

EXAMPLE C: ONE-DIMENSIONAL CREEP TEST

A second long-term creep test was conducted in a one-dimensional consolidometer on the same undisturbed deep sea clay as used in the triaxial test. The sample was loaded to three different stress levels for a total of 158,406 min (110 days). Initially the sample was loaded to 1·8 kPa, followed by increases to 4·3 kPa at 43,190 min (30 days) and to 8·9 kPa at 81,940 min (57 days). In contrast to deviatoric loading of the triaxial specimen, each of these loads was applied in one

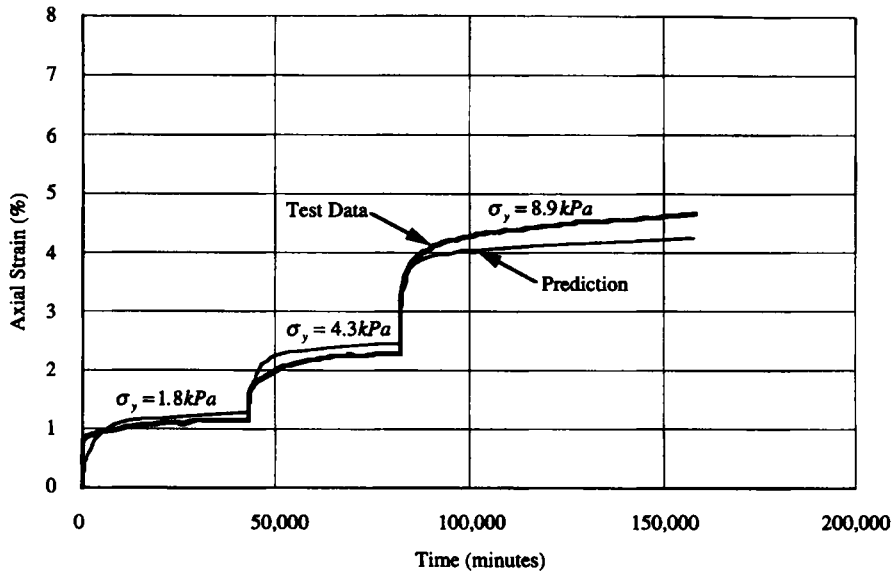

Figure 10. Comparison between 1-D creep test and GEO-CP prediction

increment. Deformation was monitored at regular intervals using dial gauges accurate to 0·0001 in. Porous stones at the top and bottom allowed for double drainage conditions.

Given the one-dimensional nature of the problem, considerably fewer elements are necessary to model the 6·5 cm (2·55 in) wide by 1·90 cm (0·76 in) high specimen. Due to symmetry, only the upper right-hand quadrant is discretized, using 12 elements as shown in Figure 3. Again, we use axisymmetric four-noded isoparametric elements with corner pore pressure nodes for a total of 78 degrees of freedom. Drainage occurs through the top by specifying zero excess pore pressures at all times at the upper boundary. All other boundary conditions are as implied in Figure 3. Time increments ranged from 1 min at the start of each stress stage to 6000 min at the end. A total of 395 increments and a minimum of five iterations per increment were used. Creep strains were calculated using Singh–Mitchell's equation (12).

The material properties used for the predictions were the same as those in Table II, except for a permeability of 10^{-7} cm/s, which was deemed more appropriate for this particular specimen. The initial stress conditions can be calculated as illustrated in Figure 9. Consolidation data indicates that the vertical preconsolidation stress is 11·8 kPa. Thus the three-dimensional preconsolidation stress p_c can be estimated from (2) as follows:

$$p = \frac{2(K_0 \times 11{\cdot}8) + 11{\cdot}8}{3} = 7{\cdot}9 \text{ kPa}$$

$$q = (K_0 \times 11{\cdot}8) - 11{\cdot}8 = 5{\cdot}9 \text{ kPa} \tag{36}$$

$$p_c = \frac{(5{\cdot}9)^2/(1{\cdot}24)^2 + (7{\cdot}9)^2}{7{\cdot}9} = 10{\cdot}8 \text{ kPa}$$

where we have assumed that $K_0 = 0{\cdot}5$. This means that the sample remains overconsolidated during the first two load applications (1·8 and 4·3 kPa) and approaches normal consolidation

during the third load application (8·9 kPa). Before the first load was applied, the sample was subjected to the weight of the upper porous stone, which produced a vertical stress of 0·2 kPa. If we assume that $K_0 = 1{\cdot}0$ in the overconsolidated region, the initial stresses can be assumed as $\sigma_x = \sigma_y = \sigma_z = 0{\cdot}2$ kPa.

Test data and predictions are compared in Figure 10. Although the predicted results do not deviate from the test data by more than 10 per cent at any time, they tend to overpredict somewhat the test data during the first two stress stages, where the applied stresses fall in the overconsolidated region, and underpredict it during the last step, where the total stresses are close to the preconsolidation stress. The discrepancy may be due to the sample having a slightly different set of material parameters from those assumed in Table I for the model. Laboratory test data show that there are natural variabilities from sample to sample, even for this relatively homogeneous clay. Because of the complex form of the constitutive relationship, it is difficult to predict how each individual parameter affects the combined elastic, plastic and creep response. We are now conducting a sensitivity analysis to better understand how the constitutive constants affect the overall predictions.

CONCLUSIONS

Two long-term drained creep tests on undisturbed samples of a deep sea clay were modelled with the new code GEO-CP using previously determined material properties. Good agreement is observed between test results and axial strain predictions. The triaxial example in particular demonstrates that the program appears to properly account for two-dimensional drainage and multiple stress increments. Although a finer mesh and higher-order elements would increase accuracy during the early phases of primary consolidation, the computed pore pressures and effective stress appear to be reasonable, both qualitatively and quantitatively. Given the relatively low permeability, pore pressures in the interior of the specimen initially rise above the applied stress before dissipating. Initial dissipation of excess pore pressures is slowed by creep.

A sensitivity analysis confirms that the behaviour during the early phases of deformation, after application of a stress increment, is most sensitive to the Singh–Mitchell parameters A and α, as well as the compressibility and permeability. On the other hand, the rate of deformation beyond the primary region is controlled primarily by the Singh–Mitchell parameter m. Computed displacements and stresses for cases with and without creep indicate that time dependency is an important component of the overall behaviour for this fine-grained deep sea clay, and presumably other similar marine sediments.

Recent numerical studies using GEO-CP to analyse the response of a semi-infinite slope for the case of *creep turn-on* have shown reasonable results as well.[26] We have now begun more thorough studies to analyse specific areas of the continental slope off the U.S. East Coast and in the Gulf of Mexico. Meanwhile, new laboratory tests on marine sediments are helping us to refine the constitutive model. For example, recent isotropically and anisotropically consolidated triaxial and direct simple shear creep tests, conducted for varying periods of time, appear to indicate material hardening beyond that of the constitutive model in GEO-CP.[5] These and other triaxial strength tests provide additional opportunities to compare predictions with carefully controlled laboratory data. Tests are also being contemplated on other types of materials such as organic and gas-rich sediments, sands and carbonates.

The constitutive model and formulation implemented in GEO-CP combine the most important aspects of fine-grained marine sediment behaviour, including creep and time-dependent hardening, with an accurate and efficient numerical scheme, allowing for the meaningful solution of field problems. More sophisticated and complicated constitutive models were not considered

because they either contain a large set of complex material parameters or they were not easily incorporated into the framework of time-dependent critical state plasticity. The parameters needed as input for GEO-CP can be determined using primarily conventional equipment and procedures. The good agreement between test results and predictions lends confidence to the overall capabilities of the program, particularly for quasi-static long-term applications on the continental slope and rise.

REFERENCES

1. H. G. Brandes, 'The drained triaxial creep behavior of deep sea clays', *M.S. Thesis*, University of Rhode Island, Kingston, Rhode Island, 1984.
2. A. J. Silva, K. Moran and S. A. Akers, 'Stress–strain–time behavior of deep sea clays', *Can. Geotech. J.*, **20**, 517–531 (1983).
3. D. W. O'Leary and E. Laine, 'Proposed criteria for recognizing intrastratal deformation and creep features in marine high resolution seismic reflection profiles', *Geo-marine Lett.* (in press).
4. R. Krishnamohan, 'Stress–strain properties and stress history of marine sediments from the Gulf of Mexico, Green Canyon Area', *M.S. Thesis*, University of Rhode Island, Kingston, Rhode Island, 1990.
5. W.-M. Tian, A. J. Silva, G. E. Veyera and M. H. Sadd, 'Drained creep of undisturbed cohesive sediments', *Can. Geotech. J.*, **31**, 841–855 (1994).
6. S. A. Akers and A. J. Silva, 'Stress–strain strength properties of marine sediments from the North Pacific', *Tech. Report*, Department of Ocean Engineering, University of Rhode Island, Kingston, Rhode Island, 1980.
7. A. J. Silva and S. A. Jordan, 'Consolidation properties and stress history of some deep sea sediments', in B. Denness (ed.), *Seabed mechanics, Proc. IUTAM and IUGG Symp.*, 1984, pp. 25–40.
8. R. Siciliano, 'Constitutive behavior of isotropically and Ko consolidated marine sediments in undrained shear', *M.S. Thesis*, University of Rhode Island, Kingston, Rhode Island, 1984.
9. A Schofield and P. Wroth, *Critical State Soil Mechanics*, McGraw-Hill, New York, 1968.
10. R. I. Borja and E. Kavazanjian, 'Finite element analysis of time-dependent behavior of soft clays', *Geot. Eng. Res. Report No. GT1*, Department of Civil Engineering, Stanford University, California, 1984.
11. R. L. Kondner, 'Hyperbolic stress–strain response: cohesive soils', *J. Soil Mech. Fndts. Div. ASCE*, **89**, 115–143 (1963).
12. D. W. Taylor, 'Research on consolidation of clays', *Report Ser. 82*, Department of Civil and Sanitary Engineering, Massachusetts Institute of Technology, Boston, Massachusetts, 1942.
13. A. Singh and J. K. Mitchell, 'General stress–strain–time functions for soils', *J. Soil Mech. Fndts. Div. ASCE, SM* **1**, 21–46 (1968).
14. M. A. Biot, 'General theory of three-dimensional consolidation', *J. Appl. Phys.*, **12**, 155–164 (1941).
15. J. R. Booker and J. C. Small, 'An investigation of the statility of numerical solutions of Biot's equations of consolidation', *Int. J. Solids Struct.*, **11**, 907–917 (1975).
16. R. I. Borja, 'Linearization of elasto-plastic consolidation equations', *Eng. Comput.*, **6**, 163–168 (1989).
17. R. I. Borja and S. R. Lee, 'Cam-clay plasticity, part I: implicit integration of elasto-plastic constitutive relations', *Comput. Methods Appl. Mech. Eng.*, **78**, 49–72 (1990).
18. H. G. Brandes, 'Finite element modeling of time-dependent deformations in marine clays',. *Ph. D. Thesis*, University of Rhode Island, Kingston, Rhode Island, 1992.
19. A. M. Britto and M. J. Gunn, *Critical State Soil Mechanics via Finite Elements*, Ellis Horwood, Chichester, U.K., 1987.
20. C. W. Cryer, 'A comparison of the three-dimensional consolidation theories of Biot and Terzaghi', *Q. J. Mech. Appl. Math.*, **XVI**, 401–412 (1963).
21. D. W. Airey, 'Finite element analysis of triaxial tests with different end and drainage conditions', *Proc. 7th Int. Conf. on Comput. Methods and Adv. in Geom.*, Vol. 1, 1991, pp. 225–230.
22. R. I. Woods, 'Finite element analysis of coupled loading and consolidation', *Proc. 2nd Int. Symp. on Num. Models in Geom.*, Ghent, 1986.
23. J. H. Atkinson, J. S. Evans and E. W. Ho, 'Non-uniformity of triaxial samples due to consolidation with radial drainage', *Geotechnique*, **25**, 353–356 (1985).
24. F. Tavenas, S. Leroueil, P. LaRochelle and M. Roy, 'Creep behaviour of an undisturbed lightly overconsolidated clay', *Can Geotech. J.*, **15**, 402–423 (1978).
25. R. E. Gibson, 'Analysis of system flexibility and its effects on time lag in pore water pressure measurements', *Geotechnique*, **13**, 1–11 (1963).
26. H. G. Brandes, A. J. Silva, M. H. Sadd and G. E. Veyera, 'Stress–strain–time modeling of submarine slopes', *Proc. 8th Int. Conf. on Comp. Methods and Adv. in Geom.*, Vol. 3, 1994, pp. 2435–2445.